

Reprinted with permission from *Lasers in Materials Processing*, copyright 1983, ASM International, Materials Park, OH 44073-0002. Although this article is being used with permission, ASM did not prepare the version for Web display. For information about ASM International or the purchase of books, visit ASM International on the Web at <http://www.asm-intl.org> or call 1-800-336-5152, ext. 5900.

AMERICAN SOCIETY FOR METALS
Metals Park, Ohio 44073

Metals/Materials Technology Series

**THE EFFECTS OF LASER SHOCK
PROCESSING ON THE FATIGUE
PROPERTIES OF 2024-T3 ALUMINUM**

Allan H. Clauer, Craig T. Walters, and Stephan C. Ford
Battelle's Columbus Laboratories
Columbus, Ohio

**1983 ASM Conference on Applications
of Lasers in Materials Processing
Los Angeles, California
24-26 January 1983**

Reprinted from *Lasers in Materials Processing*, 1983, ASM, Metals Park, Ohio, pp. 7-22.

8301-002

No part of this paper may be reproduced, stored in a retrieval system, or transmitted, in any form or by any means, electronic, mechanical, photocopying, recording, or otherwise, without the prior written permission of the publisher.

Nothing contained in this paper is to be construed as a grant of any right of manufacture, sale, or use in connection with any method, process, apparatus, product, or composition, whether or not covered by letters patent or registered trademark, nor as a defense against liability for the infringement of letters patent or registered trademark.

SAN: 204-7586
Copyright 1983 American Society for Metals
All rights reserved

8301-002

**THE EFFECTS OF LASER SHOCK
PROCESSING ON THE FATIGUE
PROPERTIES OF 2024-T3 ALUMINUM**

Allan H. Clauer, Craig T. Walters, and Stephan C. Ford
Battelle's Columbus Laboratories
Columbus, Ohio

INTRODUCTION

The effects of laser shock processing have been investigated in a number of metals and alloys with increases in hardness and tensile and fatigue strengths reported (1-7). A previous study of the fatigue response of laser shocked aluminum alloy plate containing simulated fastener holes showed marked increases in fatigue life in some cases. In addition, the study suggested certain process and geometry changes which would either further enhance the fatigue property improvements or aid in understanding and controlling the laser shock phenomenon influencing the properties (7). This paper describes the effects on fatigue life resulting from several different laser beam geometries and process conditions.

Both solid beam and annular beam geometries were used. The annular beam was added to determine whether a crack could be slowed down by encountering a laser shocked region. In addition, specimens were shocked from both sides simultaneously, from both sides consecutively with a momentum trap on the unirradiated side, and from one side only with a free surface opposite the irradiated side. The purpose of the momentum trap was to minimize the effect of the reflected wave from the surface opposite the irradiated surface. The one-side only shot without the momentum trap was to enable comparison to be made between the full effect of the tensile stress wave reflected from the surface opposite the irradiated side to the effects of a once through passage of the shock wave, i.e., with the momentum trap.

To understand the observed effects on the fatigue life, surface and in-depth residual stress distributions were determined for each of the laser beam geometries and process conditions. Both the residual stress and fatigue results are presented and discussed.

EXPERIMENTAL PROCEDURES

The 2024-T351 material was received as 0.25-inch-thick plate. The T351 condition consists of a solution treatment followed by a light roll-leveling pass which introduces a small amount of deformation (approximately 1 to 2 percent reduction) and natural aging at ambient temperature. The surfaces of the momentum - trapped specimens were given a superficial grinding. All other specimens were treated and tested with the as-received surface intact.

Fatigue Testing

The fatigue specimens were prepared in accordance with Figure 1. Short, narrow notches were electrodischarge machined into the sides of the hole to act as crack initiation sites and provide a consistent crack initiation behavior. The configuration of the hole and the laser shocked zones are shown to scale in Figure 1. The outer diameter of the solid and annular shocked zones are the same. The inner diameter of the annular zone is also indicated.

The fatigue test specimens were instrumented with crack measuring gages to monitor crack initiation and crack growth rates. They were cycled in an electro-hydraulic fatigue test machine in the tension-tension mode at a maximum stress of 15 ksi and a minimum stress of 1.5 ksi, i.e., $R=0.1$.

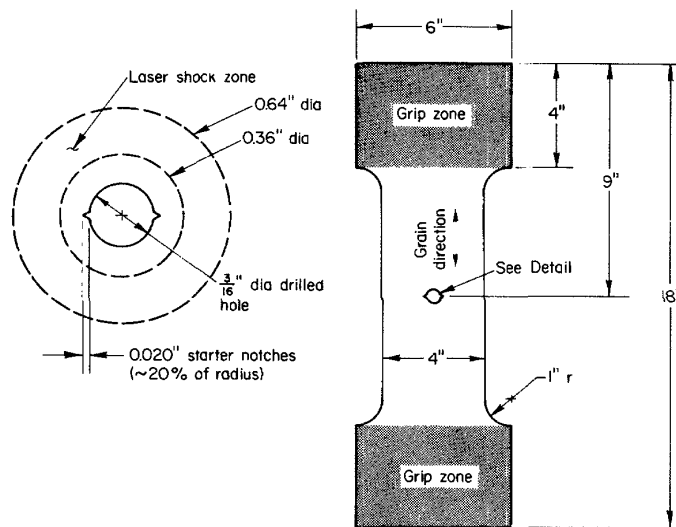


Figure 1. Fatigue Specimen and Detail of the Hole, Starting Notches, and Laser Shocked Zone. Shown here is the Annular Shaped Laser Shocked Zone; the Solid Beam is the same size as the Outside Diameter of the Annular Beam.

Laser Shock Processing

A six amplifier stage CGE high energy neodymium glass pulsed laser was used for the laser shock processing (LSP). Optics were set up to split the 200 J beam from the laser into two beams which were each routed through one additional amplifier. This arrangement permitted irradiations with up to 200 J per side in split beam irradiations. All laser irradiations were conducted with the eight stage laser system operating in a 30 ns pulse length mode. An aluminum coated plastic film (blow-off foil) was employed in the system to suppress superradiance prior to Q-switching. This method provides a sharply rising pulse (risetime less than 10 ns) which is essential to achieving significant shock pressures in the material. Beam diagnostics included a fast photodiode viewing a reflection from the central part of the beam after the sixth amplifier to provide pulse shape records, and two calibrated integrating photodiode assemblies to provide a measurement of total pulse energy per beam delivered to the target area. The energy readings were corrected for

reflection losses at the acrylic beam entrance windows to the process chamber. All beams were focused with 1 m focal length antireflection coated lenses and target placement was in front of focus in the geometric region of the beam.

Residual Stress Specimens. Square plate-type specimens (4 x 4 x 0.25 inch) were machined from the as-received plate for the residual stress study. In most specimens, a 0.187-inch-diameter hole was drilled through the center of the plate to simulate a fastener hole. Before laser processing, the work surface of the plates was spray painted with metal primer and flat black paint as an opaque overlay for laser beam absorption. The transparent overlay materials were 1.5-inch-diameter by 0.125-inch-thick disks of either fused quartz or acrylic plastic with optical quality surfaces on both sides. The discs were pressed snugly against the painted surface by a clamping ring secured to the specimen holder with screws. The specimen holder was placed in a wooden enclosure with replaceable acrylic beam entrance ports to confine the debris generated by the explosion of the overlay disc.

The processing parameters employed in the residual stress measurements are summarized in Table 1. The laser shocking geometries are shown in Figure 1. For specimens R1 through R4, an attempt was made to vary fluence in a systematic manner. As a result of uncontrolled energy variation, two specimens ended up with nearly the same fluence. Specimens R5 and R6 were irradiated with a larger beam diameter (0.64 in. as opposed to 0.45 in.) to explore possible beam size effects. Specimen R7 was identical to R5 except that no hole was present so that the effects of the hole on the residual stresses could be assessed. Specimens R8 and R9 are repeats of R1 with acrylic plastic used in place of the fused quartz overlay. All of the above described specimens employed split-beam simultaneous irradiations. Specimen R10 was similar to R7 but irradiated from one side only.

Specimens R11 and R12 were processed using new conditions. Specimen R11 was irradiated simultaneously from both sides with an annular shaped beam (0.64 in. outside diameter, 0.36 in. inside diameter) (Figure 1). The annular beam was formed by mounting a circular aluminum blocking disk on a wire spider located near the target plane with the blocking disk axis coaligned with the axis of both the beam and the drilled hole.

Table 1. Laser Shock Processing Parameters for Aluminum
2024-T351 Residual Stress Samples

Specimen Number	Hole Diameter, in.	Beam Diameter, in.	Symmetry (a)	Overlay	Average Fluence, J/cm ²		Pulse Width, ns	Peak Power Density, 10 ⁹ W/cm ²	
					Side 1	Side 2		Side 1	Side 2
R1	0.19	0.45	BS	quartz	~160	~160	~13	~12	~12
R2	0.19	0.45	BS	quartz	134	139	15	8.9	9.3
R3	0.19	0.45	BS	quartz	134	129	15	8.9	8.6
R4	0.19	0.45	BS	quartz	98	96	14	7.0	6.9
R5	0.19	0.64	BS	quartz	~77	~78	~13	~5.9	~6.0
R6	0.19	0.64	BS	quartz	69	66	13	5.3	5.1
R7	none	0.64	BS	quartz	~78	~78	13	~6.0	~6.0
R8	0.19	0.45	BS	acrylic	~160	~160	13	~12	~12
R9	0.19	0.45	BS	acrylic	150	146	15	10.0	9.7
R10	none	0.64	OS	quartz	~70	~70	~13	~5.4	~5.4
R11	0.19	0.64/0.36 ^(b)	BS	quartz	80	79	18	4.4	4.4
R12	0.19	0.64	MT	quartz	82/82 ^(c)		23/26 ^(c)	3.6/3.2 ^(c)	

(a) BS = both sides, OS = one side, MT = momentum trap (two separate one-sided irradiations).

(b) Annular beam (outside diameter/inside diameter).

(c) Side 1/Side 2.

Specimen R12 explored the effect of a momentum trap. It was irradiated with sequential one-sided irradiations using a 1.63 cm diameter solid circular beam. In this case, the unirradiated surface was backed up with a spring loaded 2024-T3 aluminum disk (1-inch-diameter x 0.25-inch-thick) during LSP to trap the shock wave and minimize any effects from a reflected tensile wave. Mineral oil was used to couple the momentum trap disk to the specimen, and a tapered cone "disk-catcher" was used to ensure that momentum trapping had occurred, i.e., the momentum trap would not slap back onto the back of the specimen. Before taking the second shot in the sequence, it was necessary to sand flat the plasma-induced "halo" crater effects created on the first surface irradiated so that the momentum trap for the second irradiation could be coupled into this surface. The shocked zone was deformed to a level slightly below the surrounding area so that sanding did not disturb the processed zone. The gap between this surface and the momentum trap surface was not measured, but it was assumed that they were coupled by the mineral oil.

Fatigue Test Specimens. Six fatigue test specimens were prepared and laser shock-processed with the processing conditions in Table 2, and the processing patterns in Figure 1. All specimens were processed with fused quartz overlays. Fatigue Specimens F1 and F2 were duplicate specimens processed with the standard solid split beam geometry. The fluence level was near 80 J/cm² with conditions similar to those of Specimens R5 and R6. Specimens F3 and F4 were annular beam processed with conditions similar to those of residual stress Specimen R11. Specimens F5 and F6 were momentum trap specimens with processing sequences similar to those for residual stress Specimen R12 except that Specimen F6 was not sanded between processing the opposite sides of the specimen.

Table 2. Laser Shock Processing Parameters for Aluminum 2024-T351 Fatigue Specimens

Sample Number	Beam Diameter, in.	Symmetry ^(a)	Overlay	Average Fluence, J/cm ²		Pulse Width, ns	Peak Power Density, 10 ⁹ W/cm ²	
				Side 1	Side 2		Side 1	Side 2
F1	0.64	BS	quartz	81	80	~15	~5.4	~5.3
F2	0.64	BS	quartz	75	75	15	5.0	5.0
F3	0.64/0.36	BS	quartz	82	78	17	4.8	4.6
F4	0.64/0.36	BS	quartz	84	78	23	3.6	3.4
F5	0.64	MT	quartz	85/86 ^(b)		23/24 ^(b)	3.7/3.6 ^(b)	
F6	0.64	MT	quartz	91/87 ^(b)		20/20 ^(b)	4.6/4.4 ^(b)	

(a) BS = both sides, MT = momentum trap (two separate one-sided irradiations).

(b) Side 1/Side 2.

The residual stresses were measured using the two Inclined Angle X-ray diffraction technique. The conditions used chromium K-alpha radiation diffracted from (311) planes of the 2024 aluminum. Diffraction peak angular positions were determined employing a five-point parabolic regression procedure after correction for the Lorentz-polarization and absorption effects, and for a linearly sloping background intensity. Details of the diffractometer fixturing are outlined below:

- Incident Beam Divergence: 1.0 deg.
- Receiving Slit : 0.5 deg.
- Detector : Si(Li) set for 90 percent acceptance of the chromium K-alpha energy
- Counts per Point : 10,000
- Psi Rotation : 0.0-45.0 deg.
- $E/(1 + \nu)$ 2024-T351 aluminum : $7.8 \pm 0.07 \times 10^6$ psi
- Irradiated Area : 0.05 x 0.10 in. (long axis aligned in the tangential direction of measurement)

The value of the single crystal elastic constant $E/(1 + \nu)$ (where E is Young's Modulus and ν is Poisson's ratio) for the crystallographic direction normal to the (311) planes of the 2024-T351 aluminum FCC lattice was determined experimentally in the course of the investigation by loading a simple rectangular 2024-T351 beam in four-point bending on the diffractometer and determining the change in the lattice spacing of the (311) planes as a function of applied stress determined by strain gages attached to the beam. The shape of a plot of the change in lattice spacing, d, as a function of applied stress was determined by linear least square regression. The single crystal elastic constant $E/(1 + \nu)$ in the [311] direction was then determined from the slope of a plot of the change in d(311) as a function of applied stress.

Material was removed for subsurface measurement of stress by electropolishing in nitric acid-methanol electrolytes to minimize alteration of the subsurface residual stress distribution. All data obtained as a function of depth were corrected for the effects of penetration of the radiation employed for residual stress measurement into the subsurface stress gradient, and for the stress relaxation which occurred as a result of the material removal.

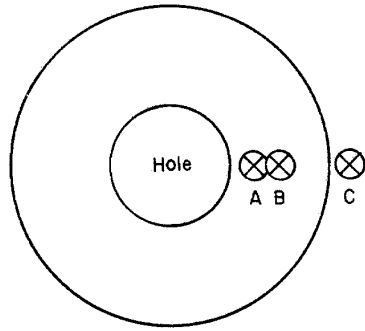
RESULTS

The residual stress results are shown in Tables 3 to 8 and Figure 2 to 10. The residual stresses were measured at three sites in some specimens, while less extensive measurements were made in other specimens only to illuminate any similarities or differences due to process changes. The locations on the specimen surfaces at which X-ray diffraction stress measurements were made are shown in Figure 2. The in-depth measurements were made successively at these same locations after electropolishing away a surface layer.

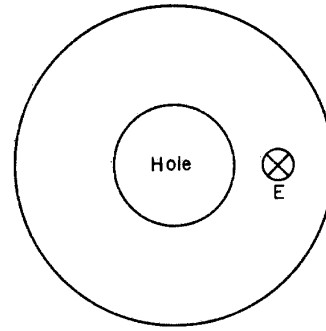
Table 3. Residual Stress Results for Standard Split Beam Laser Shock Processing Around a Drilled Hole with a Fused Quartz Overlay

Specimen Number	Power ^(a) Density, W/cm ²	Depth Below Surface, in.	Residual Stress, ksi			
			Location of Measurement			
			A	B	C	D Unshocked
R1	12, 12 X 10 ⁹	0.000	-37.5	-47.5	8.3	-8.0
		0.002	-45.4	-45.1	4.1	-4.5
		0.007	-33.1	-31.3	-3.9	-5.6
		0.012	-27.0	-25.2	2.6	-2.5
		0.022	-16.3	-11.6	0.8	-1.3
R2	8.9, 9.3 X 10 ⁹	0.000		-52.7		-9.4
		0.002		-50.4		-4.0
		0.006		-45.5		-11.8
		0.015		-34.4		-1.3
		0.025		-16.9		-0.9
		0.035		-14.7		-4.1
R4	7.0, 6.9 X 10 ⁹	0.043		-6.4		-2.8
		0.000	-43.2	-57.3	-10.7	
		0.004	-43.7	-46.8	-25.8	
		0.008	-31.5	-46.2	-18.9	
		0.012	-33.1	-39.6	-3.0	
R5	5.9, 6.0 X 10 ⁹	0.023	-26.4	-24.9	-7.4	
		0.000		-58.9		
		0.002		-44.8		
		0.008		-33.9		
		0.012		-32.4		
		0.032		-11.7		
		0.044		-10.5		
		0.052		-9.5		

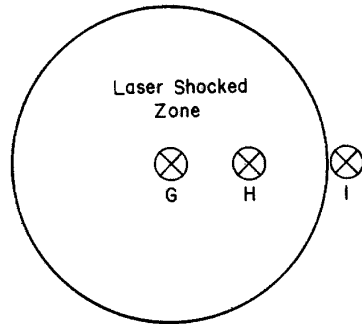
(a) The power density on each side of the specimen is shown: Side 1, Side 2.



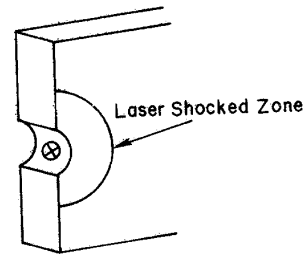
a. Drilled hole, specimens R1, R4, and R8



b. Drilled hole, specimens R2, R5, and R9



c. No hole, specimens R7 and R10



d. One side of drilled hole, specimens R3 and R6

Figure 2. Locations of the Residual Stress Measurements for the Various Specimen and Process Geometries. The Annular Beam Locations are shown in Figure 8.

The variation of the surface residual stresses across the radius of the laser shocked zone can be determined from the two specimens having no drilled hole (Specimens R7, R10). The results are shown in Figure 3 along with previous results on 7075-T6 using a water overlay (7). Each material shows a lower surface residual compressive stress in the center of the laser shocked region, a maximum at about halfway between the center and edge, and a tensile stress near or outside of the laser shocked zone. The lower value at the center of the spot is not understood. It is doubtful that it results from a lower beam intensity in the center of the beam. Rather, it may result from the elastic-plastic constraints of the material response.

Influence of Power Density. The residual stresses for the split solid beam irradiation at different power density levels are shown in Figure 4. These data are taken from Specimens R1, R2, R4, and R5, all of which had the hole drilled before shocking and used fused quartz transparent overlays. The readings all represent the region midway between the edge of the hole and the edge of the laser shocked zone (locations B. in Figures 2a and 2b, and H in Figure 2c). Additional results for Specimen R7 without a drilled hole are shown in Table 5. The residual stresses in the as-received condition, unshocked, show a small surface residual compressive stress of about -8 ksi extending to slightly greater than 0.020 in. below the specimen surface. All the laser shocked conditions developed surface stresses of -27 to -59 ksi to projected depths of 0.040 in. or more. The compressive stress profile in Specimen R7 (Table 5) at location H is similar to that of Specimen R5 at the same power density in Figure 4. The trend of the magnitude of the surface stress with power density is shown in Figure 4b. Surprisingly, there is a linear increase in the magnitude of the compressive stress with decreasing power density. Included in Figure 4b is the result from the mid-point of the annular shaped laser shocked zone (Specimen R11, Location D in Figure 8). This specimen was processed at the lowest power density and its residual stress level is consistent with the trend in the solid beam data. Eventually, at still lower power densities, the magnitude of the surface compressive stresses must begin to decrease.

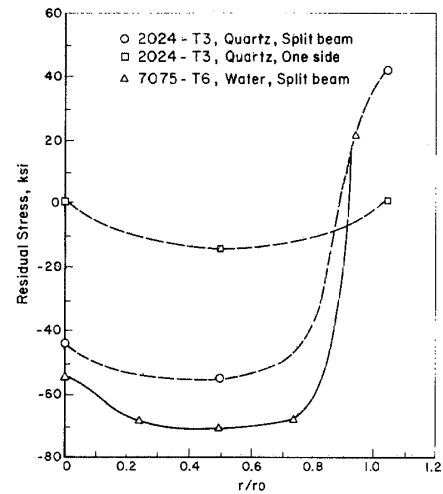
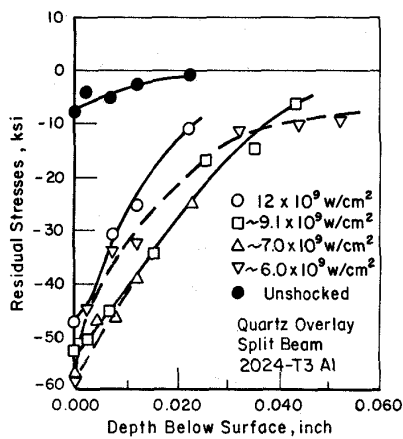
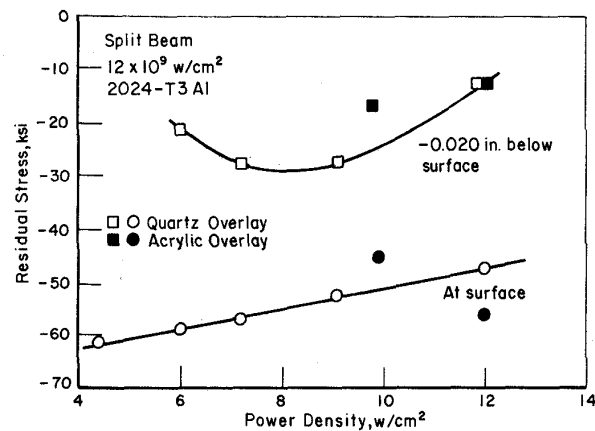


Figure 3. Variation of the Surface Residual Stress Along the Radius of the Laser Shocked Zone. r_0 is the Radius of the Laser Shocked zone.



a. In-Depth Residual Stress Profiles



b. Variation of Surface Residual Stress with Laser Beam Power Density

Figure 4. Influence of Laser Beam Power Density on the Residual Stresses.

Not only the magnitude of the surface stresses, but also the depth variation of the stresses will have an effect on the crack initiation and propagation behavior. One indication of the influence of power density on the in-depth stress is shown by a plot of the magnitude of the stresses at 0.020 in. below the surface (Figure 4b). Figure 4b indicates there may exist a maximum level of compressive stress at some intermediate power density, e.g., about $8 \times 10^9 \text{ W/cm}^2$. Higher power densities produce shallower residual stresses.

Influence of a Momentum Trap. For many applications it will not be possible to have line of sight access to both sides of the fatigue critical region for split beam shocking. For this reason, a procedure for irradiating from one side only was investigated, i.e., irradiating from one side with a momentum trap placed against the other side. The momentum trap carries away the tensile wave which would produce some distortion or bulging of the plate when reflected from the free back surface of the target area.

The momentum trap was a disk of the same material as the specimen to minimize any stress wave reflections at the specimen/momentum trap interface. The 0.25 in. thickness of the trap was adequate to carry away all of the shock wave. For example, assuming the entire stress wave is not more than 200 nsec in duration and the sound speed in aluminum is $5 \times 10^5 \text{ cm/sec}$ or less, the maximum length of the stress wave would be $(200 \times 10^{-9} \text{ sec}) \times (5 \times 10^5 \text{ cm/sec}) = 1 \text{ mm} = 0.04 \text{ in.}$

The results are summarized in Table 4 and plotted in Figure 5. Compressive stresses were produced on both sides of the specimen by the successive shocking procedure. The in-depth stress profiles of the first and second sides shocked are almost identical. The first side shocked has a slightly lower surface stress, which may or may not be a result of the interaction with the second side shock wave. These results illuminate two points. Firstly, they confirm the expectation that the surface residual stresses are created at the irradiated surface by the initial passage of the stress wave into the material. Secondly, the preservation of the residual stresses on the first side shocked after laser shocking the second side demonstrates that passage of a compressive shock wave through a compressive residual stress region will not significantly change the existing residual stresses. However, this may not be true for the interaction between a residual stress field and a stress wave of opposite sign, e.g., a tensile stress wave passing through a residual compressive stress region may degrade or remove the compressive residual stresses as suggested by the one side shock results presented later.

The momentum trap produced residual stress profiles similar to those developed by the split beam, Figure 6. The $6 \times 10^9 \text{ W/cm}^2$ condition is the nearest comparable power density split beam condition. The magnitude of the surface stresses for the momentum trap condition are slightly lower than for the split beam shots, possibly because the power density is lower. If the lower surface stresses are a result only of the lower power density and no other interactions, a comparison of the -40 to -44 ksi surface stress at the $3.4 \times 10^9 \text{ W/cm}^2$ power density level of this condition to the residual stresses shown in Figure 4b indicates a sharp decrease in surface stresses below a power density of 4 to $5 \times 10^9 \text{ W/cm}^2$.

Table 4. Residual Stresses on Both Sides of a Consecutively Shocked, Momentum Trapped Specimen. Specimen R12.

First Side Shocked		Second Side Shocked	
Depth Below Surface, in.	Residual Stress, ksi	Depth Below Surface, in.	Residual Stress, ksi
0.000	-39.3	0.000	-43.9
0.002	-35.3	0.003	-33.6
0.009	-30.8	0.007	-33.3
0.014	-32.3	0.012	-23.6
0.018	-26.9	0.018	-26.0
0.028	-17.4	0.028	-18.8

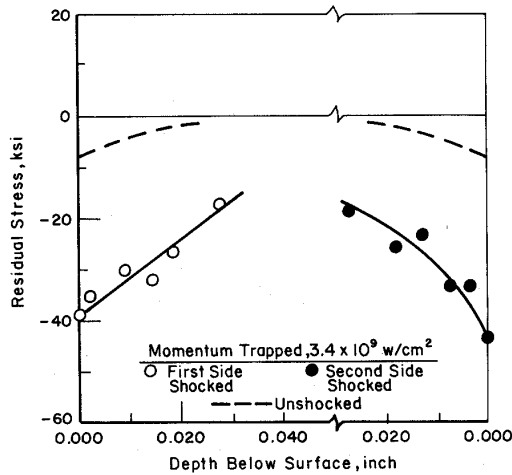


Figure 5. In-Depth Residual Stress Profiles on Both Sides of a Consecutively Shocked, Momentum Trapped Specimen. Specimen 6AB.

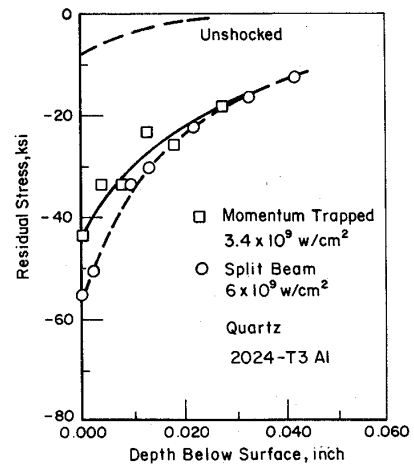


Figure 6. Comparison of the In-Depth Residual Stresses for the Split Beam and Momentum Trap Configurations.

Laser Shock from One Side Only. Another experiment to evaluate laser shocking of configurations with limited laser access to the back side was to laser shock a specimen from one side with the opposite surface a free surface (no supporting material or momentum trap was present). The results are presented in Figure 7 and Table 5. The residual stresses were measured at the locations G, H, and I (Figure 2c) on the laser shocked side, but only at locations G and H on the back side.

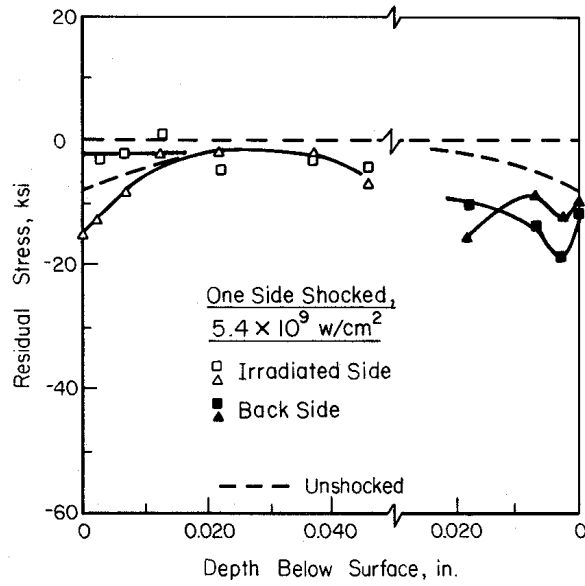


Figure 7. Residual Stress Profiles for Shocking one side only.

Table 5. Residual Stress Results for Specimens Without a Drilled Hole, Fused Quartz Overlay

Specimen Number	Power Density, W/cm ²	Depth Below Surface, in.	Residual Stress, ksi Location		
			C	H	I
R7	Split Beam 6.0, 6.0 X 10 ⁹	0.000	-43.9	-55.0	42.1
		0.002	-40.9	-50.5	7.8
		0.008	-32.6	-33.7	-4.2
		0.013	-31.2	-30.8	-11.3
		0.022	-24.0	-22.5	-9.6
		0.033	-16.2	-16.5	-12.4
		0.042	-10.7	-12.9	-6.1
R10	One Side 5.4 X 10 ⁹	<u>Laser Shock Side</u>			
		0.000	0.3	-15.0	0.8
		0.002	-3.1	-12.8	4.2
		0.007	-2.2	-8.8	-22.0
		0.013	1.0	-2.4	-19.6
		0.022	-4.9	-2.2	-9.8
		0.037	-3.3	-2.6	-9.0
		0.046	-4.5	-7.5	-8.5
		<u>Unshocked Side</u>			
		0.000	-11.8	-9.9	
0.002	-18.7	-12.8			
0.007	-13.3	-8.7			
0.018	-10.3	-15.9			

The residual stresses after laser shocking one side only (Figure 7) compared to the momentum trap (Figure 5) which was similarly shocked from one side at a time, are very different. The surface stresses on the irradiated surface of the one side only specimen are compressive but very low, about that of the unshocked material (Figure 5). The lower residual stress at the center of the laser shocked zone compared to those away from the center is consistent with the results for split beam shocking (Figure 3). There appears to be some increase in the compressive stress beyond 0.040 in. below the surface but the increase is no higher than the projected levels of the stresses at that depth for the split beam and momentum trap configurations.

The back side results are similarly surprising. The residual stresses are compressive, at levels higher than the unshocked material, and rise to a maximum at 0.002 in. below the surface before decreasing at greater depths.

From the momentum trap results, it is clear that the shocked side on the one-side shocked specimen had a significant residual compressive stress profile similar to that shown in Figure 5 after the initial shock wave had passed through the specimen. However, instead of passing out of the specimen and being carried away as in the momentum trap experiment, the shock wave reflected from the unsupported back surface as a tensile stress wave, producing the residual stress profile visible at the rear surface. However, it is not understood why the residual stresses at the back surface are compressive and not tensile as might be expected if conditions similar to those contributing to spalling were developed at this free surface.

When the reflected tensile stress wave returns to the original shocked surface, it had to have had enough amplitude to reduce the original compressive residual stresses to the levels observed in Figure 7. Previous measurements of the change in the amplitude of stress waves as they travel through aluminum showed considerable decrease in peak pressure after passage through 3 mm of aluminum (5). In the present case, the distance of travel from the irradiated surface to the back surface and return to the front surface would be 12 mm, a much longer distance, and in addition there would be a loss of amplitude through plastic interaction with the back surface as indicated by the residual stress pattern there. It might be expected that after this distance the peak stress would be at or below the dynamic yield strength of the unshocked material, i.e., the wave would be an elastic wave. The observation that it was able to modify the front surface residual compressive stresses, possible only by plastic deformation, suggests that a Bauschinger effect is operative. The Bauschinger effect is the decrease in flow stress shown by materials when the direction of plastic deformation is reversed, e.g., first in compression, then in tension. This phenomenon would explain the elimination of the shocked side residual compressive stresses by the reflected tensile stress wave.

If the reflected tensile wave is the cause for the low compressive residual stresses at the shocked surface, then there are many applications where surface residual compressive stresses can be created and retained by shocking one side only. One of these is in thicker specimens where the amplitude of the ringing elastic wave has decayed below the Bauschinger yield stress of the compressed material by the time it returns to the shocked surface. This effect is supported by recent results in thick steel specimens (8). Another is where the rear surface is not a flat reflecting surface. For example, in applications such as keyways and fillets in shafts and machine or structural parts, the rear surface may be cylindrical or highly irregular. These non-flat surface

configurations will cause the reflected tensile wave to be diffuse making it unable to modify the front surface residual stresses.

Influence of Annular Shaped Shocked Region. Another approach was explored for the purpose of modifying crack initiation and propagation to render the cracks visible on the sheet surface soon after initiation (avoid crack tunneling) (7) but still inhibit crack propagation. This was an annular shaped shocked region which allowed the crack to initiate and grow from the starter notch similar to an unshocked specimen, but to later encounter a region of residual stress which would slow the propagation rate. This annular beam was configured to the hole as shown in Figure 1 and the split beam arrangement was used. The results for the residual stresses are presented in Table 6 and Figures 8 and 9.

Table 6. Residual Stresses in a Specimen Shocked With an Annular Beam. Specimen R11(a).

Depth Below Surface, in.	Residual Stress, ^(b) ksi					
	A	B	C	D	E	F
0.000	-23.3	-34.0	-64.5	-61.1	-56.2	41.8
0.003	-22.8	-34.0	-53.3	-52.3	-47.8	1.9
0.008				-46.1		
0.012	-16.8	-17.4	-34.2	-42.1	-32.1	-20.5
0.022				-25.6		
0.033				-24.1		

(a) Power density = 4.4×10^9 w/cm².

(b) The lettered locations correspond to those shown in Figure 8.

The results show that even in the unshocked region around the hole, there is a significant increase in the compressive residual stresses. The magnitude of the residual stress rises to a maximum across the laser shocked region itself (Figure 9). The surface stresses are even higher than those observed with the solid beam. However, there was some non-uniformity of the beam intensity around the annular region and the residual stresses were measured in a region that showed a significant depression of the laser shocked region; an indication of the highest power density in this region.

Immediately outside the laser shocked zone, a residual tensile stress should be present to compensate the compressive stress. In the case of Specimen R11, the tensile stress extends only a few thousandths of an inch below the surface before it becomes compressive. A similar result was found in Specimen R7 (Location I, Table 5, but not in Specimens R1 or R4 (Location C, Table 3). The measured stresses in this region may be quite sensitive to the location of the X-ray beam just inside or outside the edge of the laser- spot.

The residual stresses extending beyond the laser shocked zone raise interesting questions. How far outside the region do these stresses extend? Is there a thickness dependence? How will these stresses affect crack initiation or propagation from nearby edges or surfaces outside the laser shocked zone? These are questions which must be addressed at some point.

Acrylic Polymer Transparent Overlay. The identification of a variety of transparent overlays is vital to the continued development of laser shock processing. The fused quartz overlay is suitable only for flat surfaces. Water is better for conforming to non-uniform surface configurations and will often be simple and quick to apply in a production situation. Another approach is to use polymeric overlays which are flexible, cheap and may even ultimately have adhesive included as an integral part of the overlay system.

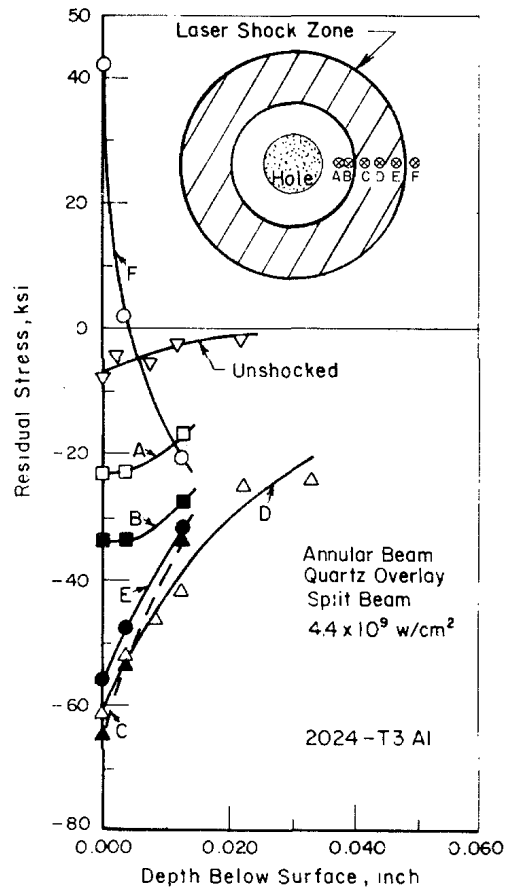


Figure 8. In-Depth Residual Stress Profiles for the Annular Shaped Beam. The Letters Designate the Positions of the Stress Measurements. Specimen R11.

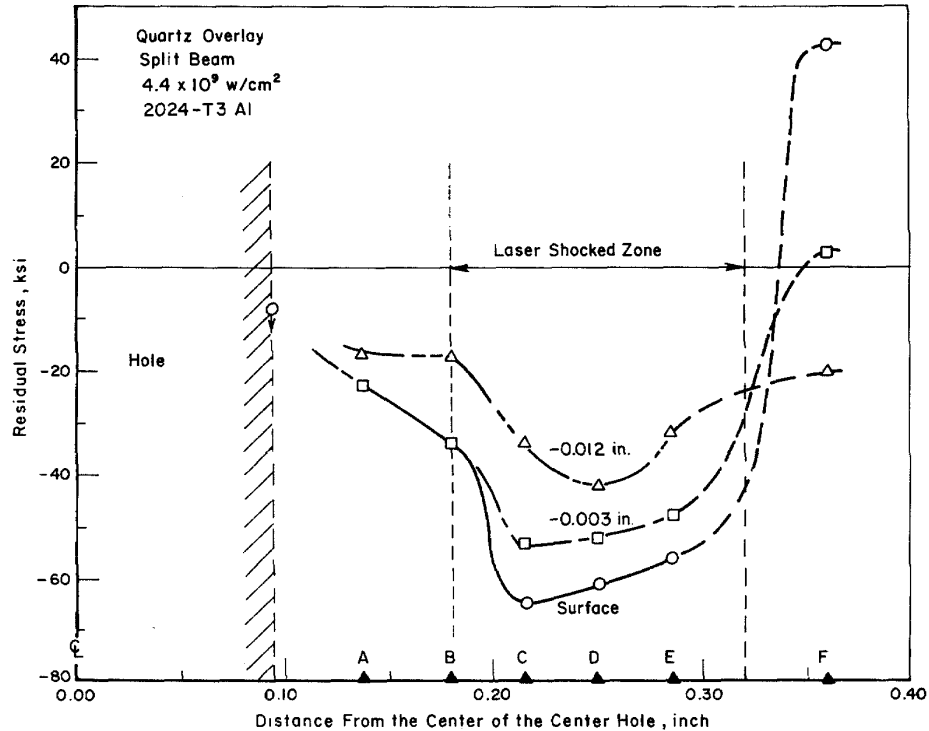


FIGURE 9. Profiles of the Residual Stresses Along the Laser Spot Radius at and Below the Surface for the Annular Shaped Beam. Specimen R11.

Two experiments were conducted using acrylic as a transparent overlay material. The results are presented in Table 7 and Figure 10. The residual stress profile midway between the edge of the hole and the edge of the laser shocked zone (Location B in Figure 2a) are shown in Figure 10. Two aspects of these profiles are noteworthy. The magnitudes of the surface stresses are comparable to those obtained with the fused quartz overlays. However, a comparison included in Figure 4b shows that there may be more scatter in these results or else that the surface stress may have a much different dependence on power density than was obtained for fused quartz. In addition, the residual stresses for the acrylic overlay may fall off more rapidly below the surface than for most of the split beam or momentum trap results using the fused quartz overlay. The stress gradient for both power densities is very similar to that of the $12 \times 10^9 \text{ W/cm}^2$ shot for the fused quartz overlay (Figure 4a), showing extrapolations to zero residual stress at 0.030 to 0.050 in. below the surface. This may be caused either by the stress waves being of shorter duration at very high power densities or by a characteristic of the acrylic overlay itself. The shorter duration stress waves could be caused in either case by the formation of a reflecting plasma during the irradiation which uncouples the beam from the blow-off material. The peak pressure of shorter duration stress waves may be lower and attenuate more rapidly than that of longer duration stress waves.

Table 7. Residual Stress Results for Standard Split Beam Laser Shock Processing Around a Drilled Hole with an Acrylic Overlay.

Specimen Number	Power ^(a) Density, W/cm ²	Depth Below Surface, in.	Residual Stress, ksi		
			A	B	C
R8	12, 12 X 10 ⁹	0.000	-48.5	-59.7	4.4
		0.002	-41.7	-43.7	-11.8
		0.006	-33.3	-31.3	-6.8
		0.012	-26.3	-28.5	-11.1
		0.022	-8.0	-9.9	-3.2
R9	10.0, 9.7 X 10 ⁹	0.000		-45.6	
		0.002		-37.6	
		0.007		-30.5	
		0.012		-22.1	
		0.022		-17.1	
		0.034		-7.2	
		0.044		-0.1	

(a) The power density on each side of the specimen is shown: Side 1, Side 2.

In-Hole Residual Stresses. It is possible that laser shocking around fastener holes might actually decrease the cycles to crack initiation at the side of the hole at mid-thickness (7), if residual tensile stresses were created at mid-thickness to compensate for the surface compressive stresses. Since crack initiation as well as crack propagation can influence fatigue life, it was necessary to establish what stress conditions were developed at the crack initiation sites on the hole surface by LSP.

For this purpose, specimens containing drilled holes were laser shocked with the standard solid, split beam using fused quartz overlays. Both laser shocked and unshocked specimens were then cut in half along the diameter of the holes. The residual stresses were then measured at the mid thickness region of the sheet on the surface of the hole and at two in-depth levels below the original surface.

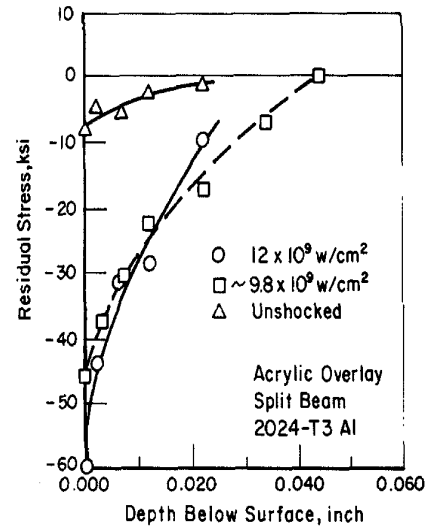


Figure 10. Residual Stress Profiles for the Acrylic Transparent Overlay at two Power Densities.

The results for the stress component normal to the sheet thickness direction (the stress tangential to the hole surface) are shown in Table 8 for Specimens R3 and R6. Specimen R3 was irradiated with a smaller spot size and a higher power density compared to Specimen R6 (Table 1). The as-drilled hole surface shows a near zero surface residual stress which drops to a small compressive stress extending to as far as 0.012 in. from the hole surface. Laser shocking definitely changes the residual surface stress to between 10 and 20 ksi compression to depths at least 0.012 in. away from the hole surface. When these results are compared to the in-depth stresses below the laser

irradiated surface there is a consistency between the two. The component of stress measured in the hole surface is the same stress as the tangential component measured in the laser shocked surfaces. For equivalent power densities some of the in-depth compressive stress profiles measured below the laser shocked surfaces (Figure 3) appear to extend well below the shocked surface, although at a low stress level. In these cases, the low level compressive residual stresses may extend completely through the thickness as suggested by the results from the hole surfaces.

Table 8: Residual Stresses on the Surface of the Drilled Holes at the Mid-Thickness of the Plate With and Without Laser Shocking.

Specimen R3		Specimen R6			
Drilled Plus Shocked		As Drilled		Drilled Plus Shocked	
Depth Below Surface, in.	Residual Stress, ksi	Depth Below Surface, in.	Residual Stress, ksi	Depth Below Surface, in.	Residual Stress, ksi
0.000	-11.2	0.000	0.2	0.000	-13.2
0.002	-14.2	0.002	-7.0	0.002	-19.6
0.006	-9.6	0.007	-3.4	0.007	-21.0
0.011	-18.3	0.012	-2.4	0.013	-24.3

The somewhat higher compressive stresses on the hole surface after laser shocking suggest that the cycles to crack initiation should be greater in the laser shocked compared to the unshocked specimens.

Fatigue Results

Fatigue crack initiation/propagation specimens were laser shocked in several conditions as described in Table 2. In addition, two unshocked specimens were tested for baseline comparisons. The fatigue life results are shown in Table 9 and the crack propagation results are presented in Figure 11. The critical crack length for this specimen configuration is about 2.2 in. Thus, the cycles at the sharp upturn in crack growth rate represents the nominal fatigue life for the specimens tested. Several reference crack lengths are indicated in Figure 11. These are a_s , the starting crack length equal to the notch root to notch root distance of the starting hole; a_{min} , the minimum crack length required to break through to the outside of the laser shocked zone, assuming the crack propagates only from one side of the hole through to the outside of the shocked zone on that side; a_{max} , the crack length required to break through the laser shocked zone if the crack propagates evenly from both sides of the hole (equal to laser shocked zone diameter); a_{ja} , the crack length required to reach the inside edge of the annular shocked zone assuming that cracks initiate and propagate evenly from both sides of the hole (equal to the inside diameter of the laser shocked region). Representative views of the fracture surfaces are shown in Figure 12 and maps of the propagating crack front contours are shown in Figure 13.

Table 9. Fatigue Crack Growth Data^(a)

Specimen Number	Laser Shock Condition	Cycles to Failure	Improvement Factors
US 1	Unshocked	50,500	1
US 2	Unshocked	49,800	1
F1	Split beam-solid spot	2,020,000	40.3
F2	Split beam-solid spot	1,340,000	26.7
F3	Split beam-annular spot	94,040	1.9
F4	Split beam-annular spot	175,830	3.5
F5	Momentum trap	720,190	14.4
F6	Momentum trap	731,150	14.6

(a) All tests conducted at 15 ksi cross section stress.
Stress Ratio $R = 0.1$.

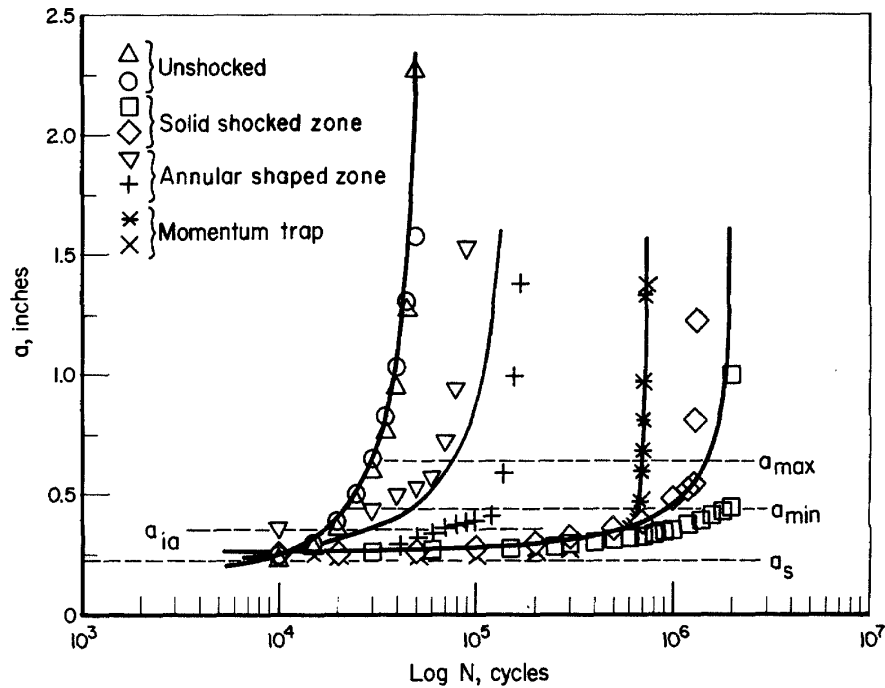


Figure 11. Crack Propagation Results for Unshocked and Laser Shocked Specimens for Different Laser Shocking Conditions Where the Plotted Crack Length is the Tip to Tip Crack Length From Both Sides of the Hole. The various meanings of a are described in the text.

The unshocked specimens have the shortest fatigue life and also the fastest crack propagation rates for all crack lengths less than the minimum length necessary to break through the laser shocked zone, a_{min} (Figure 11). For the laser shock conditions, the split-beam annular shaped shocked zone showed a fatigue life of 2 to 3.5 times greater than the unshocked conditions while

the momentum trapped specimens showed increases of 14.5 and the split-beam solid shocked zone showed an increase of 27 to 40 times (Table 9).

The life improvement for the solid split beam is nearly an order of magnitude greater than the improvement obtained in an earlier program (7). This is probably attributable to several differences in the laser shocking conditions used in this program compared to the previous one, i.e., different transparent overlays (fused quartz overlay vs. water overlay), slightly lower power densities (5×10^9 W/cm² vs. 6×10^7 W/cm²), a different stress concentration/crack initiation configuration (EDM notch vs. a 0.081 in. radius) and a longer crack path through the laser shocked zone (0.207 vs. 0.132 in.). Each of these effects, except for the sharper notch, would significantly improve the fatigue life. The effect of the slightly lower power densities in this investigation is probably small (Figure 4b). However, the crack initiation behavior is significantly different between this investigation and the earlier one (7).

In the earlier investigation, crack initiation in the unshocked condition was reported to occur at nominally 10^5 cycles (Table A-10, Specimens 29 and 30, reference 7). This value was somewhat conjectural because of crack tunneling and the small, nearly invisible crack openings in the laser shocked zone. For both the shocked and unshocked conditions, the cracks tended to initiate at a single site on the edge of the hole in the central region of the plate thickness (7).

In this investigation the improved electrical crack monitoring method permits more confidence in the crack initiation data. Crack initiation appears to begin at 10^4 cycles or earlier (Figure 11); compare extrapolation of the a vs. N curves to the dashed line a_s . This is up to an order of magnitude earlier than the estimated crack initiation period of the previous tests (7) and is caused by earlier crack initiation at the sharper starting notch. Also, multiple crack initiation sites are visible along the length of the notch on the fracture surfaces shown in Figure 12. The edge of the notch is along the top of each micrograph. Because of early crack initiation, most of the fatigue life in this investigation was in the crack propagation mode. For the unshocked specimens crack initiation appears to be 20 percent or less of the observed life compared to possibly greater than 70 percent in the earlier program (7). In the laser shocked specimens it is an even lower percentage, less than 1 percent in some cases.

The crack growth rate of all the laser shocked specimens is much lower than that of the unshocked specimens for crack lengths less than a_{min} . Most of the laser shocked specimens had a low growth rate up to a_{min} , and then either an almost discontinuous increase in rate from a_{min} to failure or a rate similar to that of the unshocked specimens. The sharp increase in growth rate suggests that in these cases the cracks grew mostly from one side of the hole and breached the laser shocked zone at length a_{min} . Thereafter, they propagated rapidly and forced the crack from the other side of the hole to penetrate the laser shocked zone very quickly under the much higher stress concentration created by the longer crack length. This is consistent with the data showing that the specimens showing the abrupt crack acceleration also had lower apparent crack lengths at a given number of cycles compared to the specimens showing more uniformly increasing crack propagation rates. However, a comparison of the crack lengths on both sides of the hole with increasing cycles does not support this idea. In both Specimens F5 (momentum trap) and F1 (standard split beam) the cracks grew at about the same rate from both sides of the crack and the acceleration in rate would then have occurred when both cracks were 30 to 50 percent through the laser shocked zone.

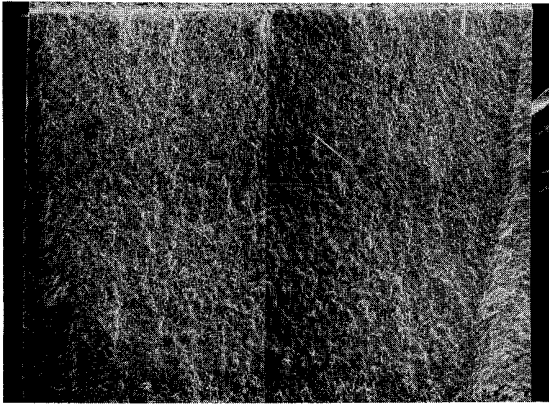
It is useful to compare the crack propagation behavior derived from the fracture surface examination for the different LSP conditions (Figures 12 and 13) and the crack growth curves (Figure 11). In the unshocked specimens, the crack front was nominally straight across the thickness of the specimen at a very early stage, and continued to propagate in this fashion as the crack grew away from the hole (Figure 13a). The split, solid beam condition shows that the surface residual compressive stresses cause the crack growth rate at the surface to lag the rate in the mid-thickness region. This slows the crack propagation rate significantly thereby increasing the fatigue life (Figure 11).

In the momentum trapped specimens, the crack front shape (Figure 13c) showed the cracks propagated differently than they did in the split beam condition. The crack front along the first side shocked, propagated ahead of the front along the second side shocked, where it propagated similar to the split beam condition. The residual surface stresses on the second side shocked were more effective in slowing the crack than was the residual stress in the first surface shocked. This difference indicates that the stress wave from the second shot modified the stress field behind the first surface shocked enough to significantly influence the crack propagation rate even though the appearance of the residual stress profiles for each surface (Figure 5) are not much different. Interestingly, the crack length measurement was made on the first side shocked in this specimen (X in Figure 11) and it showed similar crack propagation rates to the split beam shocked specimens below a_{min} . The sudden crack acceleration leading to shorter life compared to the split beam condition probably occurred when the crack on the first side shocked (left side in Figure 13c) had broken through the laser shocked zone. This is supported by the contours of the crack front in Figure 13c being drawn out almost parallel to the second side shocked by the rapid advancement along the first side shocked. If this modification of the first side stress field had not occurred, the momentum trapped specimen would be expected to have much longer fatigue lives.

Another possible contribution to longer lives after split beam shocking compared to momentum trapping may be the deformation created in the center thickness region of the plate by the superposition of the shock wave (5). This effect contributes additional cold work to the specimen mid-thickness region and possibly modifies the residual stress pattern.

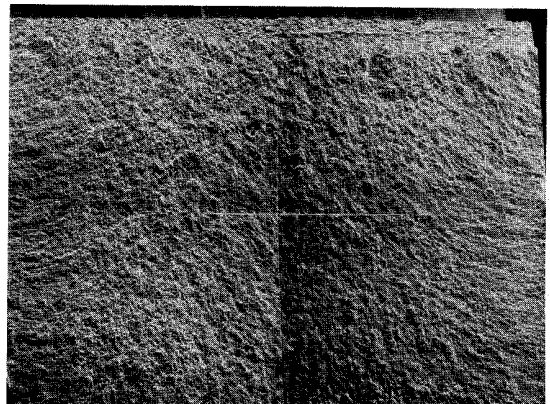
The effect of the annular shocked zone was to produce some improvement in fatigue life compared to the unshocked condition. One of the specimens appeared to show much earlier crack initiation than the other specimens (inverted triangles, Figure 11). Both specimens, but one in particular (crosses), showed the anticipated slowdown of crack propagation when the crack

Edge of Notch



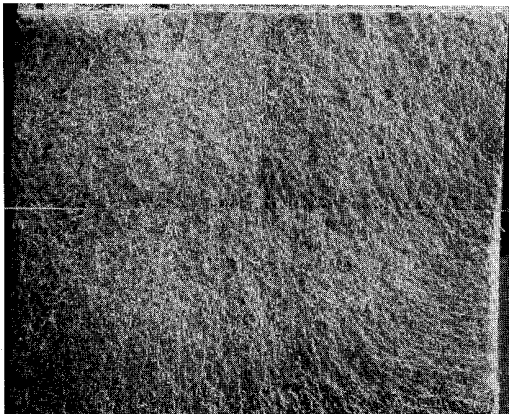
a. Unshocked condition

Edge of Notch



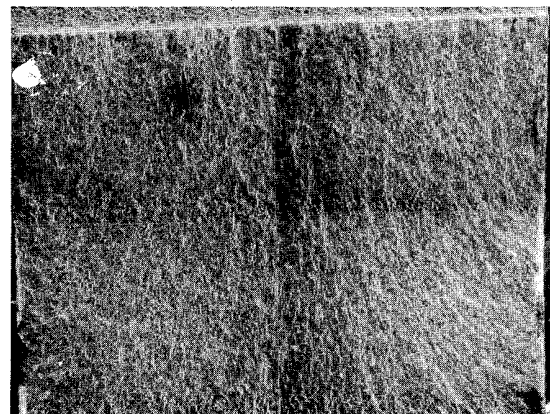
b. Laser shocked with split beam and solid spot

Edge of Notch



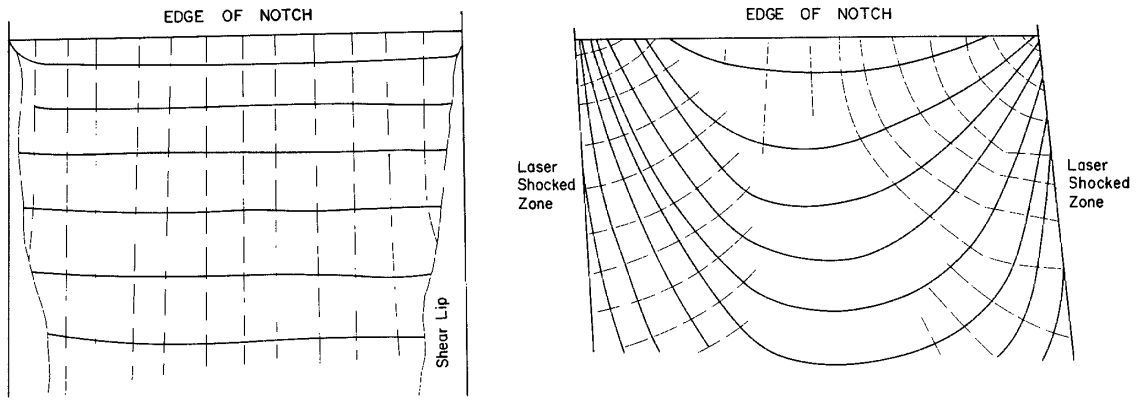
c. Laser shocked on both sides successively with a momentum trap

Edge of Notch



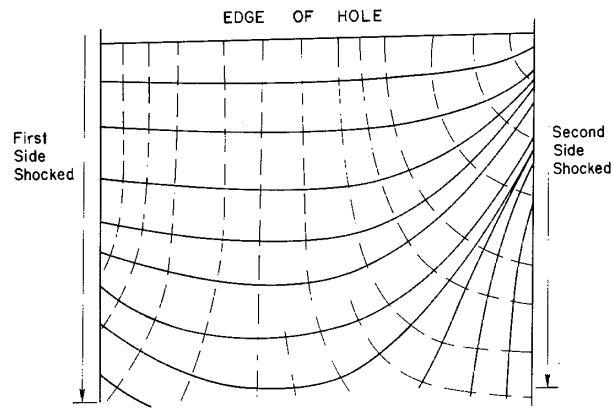
d. Laser shocked with split beam

Figure 12. Fracture Surfaces of Specimens for each Condition Fatigue Tested. The edge of the notch is located at the top of each micrograph with the crack propagating downward across the width of the specimen. Magnification: the specimen width is 0.25 in.

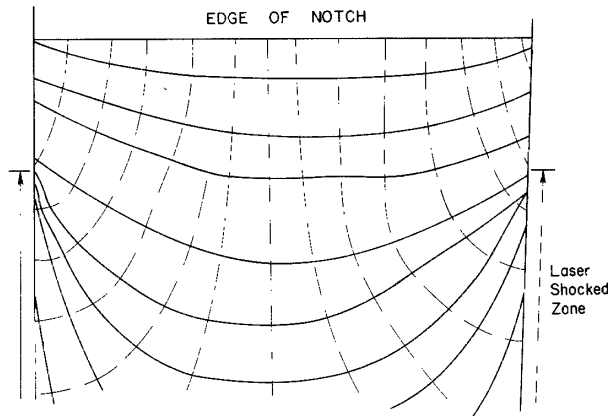


a. Unshocked condition

b. Laser shocked with split beam and solid spot



c. Laser shocked on both sides successively with a momentum trap



d. Laser shocked with split beam and an annular spot

Figure 13. Schematics of the Fracture Surfaces Shown in Figure 12 Showing the River Line Pattern Contours as Dashed Lines and successive Crack Front Contours as Solid Lines. These drawings are oriented identically to the micrographs in Figure 12.

reached the length a_{ja} , at the edge of the laser shocked zone (compare the slope indicated by the data points between a_s and a_{ja} to that between a_{ja} and a_{min}).

The fracture surfaces (Figures 12d and 13d) clearly show the effects of the residual stresses (Figures 8 and 9). The cracks initiate all along the edge of the notch and start to propagate much as in the unshocked specimen. As the crack grows and approaches the inside diameter of the laser shocked zone, the portions of the crack front intersecting the surfaces slow down through the interaction with the residual compressive stresses. At this point the crack front begins to tunnel through the mid-thickness of the specimen in the same way as in the solid split beam shocked specimens.

The annular shaped shock beam zone is effective in decreasing the crack propagation rate. With a more uniform beam intensity and improved beam shaping methods it is expected that the observed life increase of two to three times can be increased still further.

CONCLUDING REMARKS

The improvements in the fatigue life produced by laser shock processing are clearly a result of the residual compressive stresses developed in the irradiated surfaces slowing the crack propagation rate. The change in the shape of the crack front and the slowing of the crack growth rate when the crack front encounters the laser shocked zone in the annular beam LSP condition support this contention.

The compressive residual stresses initially produced below the irradiated surface can be modified or eliminated by the passage of a tensile stress wave. For this reason, if one side only shocking is used, it is necessary to either process thicker specimens to decrease the intensity of the reflected wave, use specimens with an irregular back surface to diffuse the reflected wave, or use a momentum trap.

Laser shock processing is a very effective method of increasing fatigue life in aluminum by treating fatigue critical regions. It is not known what effect the tensile residual stresses surrounding the laser shocked region would have on crack initiation. A previous study of the effect of LSP on fatigue of welded aluminum specimens used a series of overlapping spots to cover the weld and heat affected zones. Significant increases in fatigue life were observed for these specimens, indicating that this effect may not be a serious problem (6).

REFERENCES

1. B. P. Fairand, B. A. Wilcox, W. J. Gallagher, and D. N. Williams, J. Appl. Phys., Vol. 43, p. 3893-3895 (1972).
2. A. H. Clauer, B. P. Fairand, and B. A. Wilcox, Met. Trans. A., Vol. 8A, p. 119-125 (1977).

3. A. H. Clauer, B. P. Fairand, and B. A. Wilcox, *Met. Trans. A.*, Vol. 8A, p. 1871-1876 (1977).
4. B. P. Fairand and A. H. Clauer, *J. Appl. Phys.*, Vol. 50, p. 1497-1502 (1979).
5. A. H. Clauer and B. P. Fairand, Applications of Lasers in Materials Processing, ed. by E. Metzbower, American Society for Metals, Metals Park, Ohio (1979).
6. A. H. Clauer and J. H. Holbrook, and B. P. Fairand, Shock Waves and High Strain Rate Phenomena in Metals, ed. by M. A. Meyers and L. E. Murr, Plenum Press, New York (1981), p. 675-702.
7. S. C. Ford, B. P. Fairand, A. H. Clauer, and R. D. Galliher, Investigation of Laser Shock Processing, Final Report, AFWAL-TR-80-3001, Vol. II (August, 1980).
8. A. H. Clauer, C. T. Walters, and S. C. Ford, to be published.